TUDelft

Delft University of Technology

A study of the elastic moduli and chemical composition of corrosion product naturally-generated due to chlorides through nano-indentation and energy dispersive X-ray spectrometry (EDS)

Rossi, E.; Zhang, Hongzhi; Nijland, Timo G.; Copuroglu, Oguzhan; Polder, R.B.; Šavija, B.

Citation (APA)
Rossi, E., Zhang, H., Nijland, T. G., Copuroglu, O., Polder, R. B., & Šavija, B. (2021). A study of the elastic moduli and chemical composition of corrosion product naturally-generated due to chlorides through nano-indentation and energy dispersive X-ray spectrometry (EDS). In G. Ye, H. Dong, J. Liu, E. Schlangen, & C. Miao (Eds.), *4th International Rilem Conference on Microstructure Related Durability of Cementitious Composites: Microdurability 2020* (pp. 431-439). Delft University of Technology.

Important note
To cite this publication, please use the final published version (if applicable).
Please check the document version above.

A STUDY OF THE ELASTIC MODULI AND CHEMICAL COMPOSITION OF CORROSION PRODUCT NATURALLY-GENERATED DUE TO CHLORIDES THROUGH NANO-INDENTATION AND ENERGY DISPERSIVE X-RAY SPECTROMETRY (EDS)

Emanuele Rossi (1), Hongzhi Zhang (2), Timo G. Nijland (3), Oğuzhan Çopuroğlu (1), Rob B. Polder (4) and Branko Šavija (1)

(1) Delft University of Technology, Faculty of Civil Engineering & Geosciences - Department of Materials & Environment, Stevinweg 1, 2628 CN Delft, The Netherlands

(2) Shandong University, School of Qilu Transportation, 25002 Jinan, , PR China

(3) TNO Buildings, Infrastructures and Maritime, PO Box 155, 2600 AD Delft, The Netherlands

(4) RPCP, Fluwelensingel 106, 2806 CH Gouda, The Netherland

Abstract

An important input parameter for numerical models that simulate cracking of the concrete cover due to reinforcement corrosion is the Elastic modulus of corrosion product (E_{cp}). Despite its relevance, E_{cp} is subject of significant variations according to the values reported in the literature, which vary from less than 100 MPa up to 360 GPa. Furthermore, E_{cp} values proposed in most of the present literature are representative of the corrosion product generated by anodic accelerated corrosion or extracted from the steel/concrete interface (SCI), which might differ from that formed in real corroding structures. Therefore, this study aims to investigate the Elastic modulus of naturally-generated corrosion product present at the SCI through nano-indentation conducted on six reinforced concrete polished sections. The polished sections were obtained from six 20-year-old reinforced concrete prisms cast with different cement type (CEM I, CEM II/B-V, CEM III/B, CEM V/A), same water/binder ratio (0.55) and which were previously exposed to NaCl solution wet/dry cycles. This study revealed that the range of E_{cp} did not considerably vary between corrosion products formed in different concrete mixes. However, corrosion product was microscopically found to consist of overlapping bands with different E_{cp}, varying for up to around 70 GPa between each other. Through Environmental Scanning-Electron Microscopy (ESEM) and Energy Dispersive X-ray Spectrometry (EDS) analysis of the indented locations, it was found that E_{cp} is highly dependent on the presence of interfacial cracks and inversely proportional to the concentration of Si and Ca, representative for corrosion product mixed with the surrounding concrete.

Furthermore, higher concentration of Fe leads to higher E_{cp}. Based on this study, an average range of values for E_{cp} between 80-100 GPa can be suggested for use in numerical models for corrosion induced cracking, regardless of cement type of the structure under investigation.
Keywords: nano-indentation, corrosion products, reinforcement corrosion

1. INTRODUCTION

Chloride-induced corrosion of reinforcement is one of the major degradation mechanisms affecting reinforced concrete structures. It involves the dissolution of iron due to ingress of harmful agents from the outside environment, which penetrates the concrete matrix and reach the reinforcement. In presence of oxygen and an electrolyte, formation of corrosion products (i.e. iron oxides and hydroxides) occurs, which generate tensile stresses inside the matrix that cause cracking of concrete, whilst reducing the effective cross-section of the reinforcement itself. Cracks enable harmful ions (such as chloride ions) to penetrate the structure more easily and accelerate the steel corrosion rate [1]. When occurring in practice, corrosion results in unforeseen maintenance and repair costs and, eventually, in faster structural failures. Therefore, predicting the cracking of concrete due to corrosion is an important topic, as suggested by the number of relevant numerical models proposed during the last decades to assess the mechanical and durability consequences of corrosion [2-6]. In these models, the elastic modulus of corrosion product (E_{cp}) is an important parameter to accurately predict the cracking time of the concrete cover since corrosion products at the steel/concrete interface (SCI) participate in the mechanical interaction between reinforcement and concrete when corrosion occurs [7]. Depending on the model, the used E_{cp} can have significant impact on the accuracy of the predicted time to cracking [8].

Many studies have been conducted to determine the most likely value of E_{cp} to be used in concrete cracking models. However, the values of E_{cp} proposed in the literature vary up to a factor of 10^6, as already pointed out by other researchers [7-8]. Furthermore, the dependency of E_{cp} on the chemical composition of corrosion products naturally-generated in different concrete mixes has rarely been investigated. Therefore, the aim of this study is to investigate the mechanical properties of corrosion products formed at the SCI in different concrete mixes and to evaluate the relation between E_{cp} and corresponding elemental concentrations of individual corrosion products through ESEM (Environmental Scanning Electron Microscope) observations and EDS (Energy Dispersive Spectrometry) semi-quantitative spot analysis.

2. MATERIALS AND METHODS

2.1 Specimen preparation

In this study, six reinforced concrete polished sections have been analyzed through nano-indentation, ESEM observations and EDS elemental mapping and spot analysis. The polished sections were obtained from 20-years-old prisms cast in 1998 by Polder et al. [9]. The prisms were cast with four different cement types (CEM I, CEM II/B-V, CEM III/B, CEM V/A), same water/binder ratio (0.55) using siliceous river sand and gravel with a maximum diameter (D_{max}) of 8 mm as aggregate. After casting, prisms were exposed to 3% NaCl solution wet/dry cycles for 6 months and otherwise left directly exposed (unsheltered) to the outside environment in Delft, the Netherlands.

One core of 20 mm in diameter was drilled from each prism parallel to the reinforcement and containing one steel bar, as described elsewhere [10]. The steel bar had 10 mm of cover depth. The cores were vacuum impregnated with fluorescent epoxy and carefully sawn perpendicularly to the bars, obtaining one 5-mm-high section per each core which was then grinded and polished prior to microscopic analysis. The composition and label of each polished section are summarized in Table 1.

Table 1: Specimen label and cement type (w/c = 0.55; D_{max} = 8 mm)

Specimen label	1550-S1	1550-S3	2550-S3	3550-S2	5550-S1	5550-S2
Cement type	CEM I	CEM I	CEM II/B	CEM III/B	CEM V/A	CEM V/A

2.2   Nano-indentation, Environmental scanning Electron Microscopy (ESEM) and Energy Dispersive Spectroscopy (EDS) analysis

Nano-indentation was conducted on the corrosion product formed at the SCI with an Agilent Nano Indenter G200 with diamond Berkovich tip (i.e. a three-side pyramidal diamond). Each polished section was subjected to one grid-like series of 100 indents (5 rows and 20 columns), with spacing between each indent of 20 μm. E_{cp} was determined through the Continuous Stiffness Method (CSM) developed by Oliver and Pharr [11]. The output E_{cp} was the average of the values measured between 1000 nm and 1800 nm in depth, while the Poisson's ratio of corrosion product was set at 0.25 [7-8].

For the microanalysis of the indented corrosion products, a Philips XL30 ESEM in hi-vac chamber conditions was used. Backscattered electron (BSE) images were acquired at 20 kV. To investigate the relation between the chemical composition and E_{cp}, EDS semi-quantitative spot analysis was conducted for around 25 spots of indented corrosion product for each specimen. For each spot, X-rays spectra were collected for 60 seconds. The spots analyzed through EDS coincided to the circular portion of corrosion product passing through all the three vertices of the triangular indenter's footprint, as graphically shown in Figure 1.
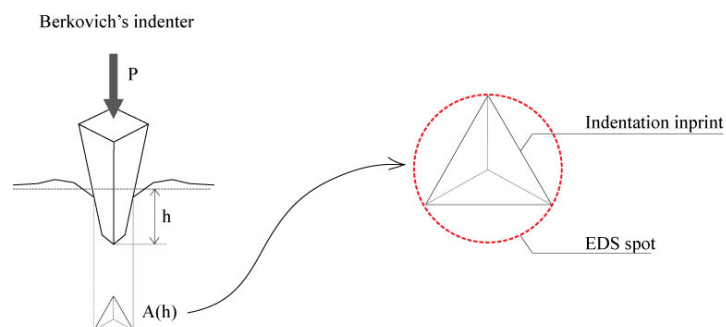

Figure 1: (left) footprint of Berkovich's indenter (P=applied load; h=penetration depth; A=inprint surface); (right) EDS spot around indenter's footprint.

3. RESULTS

In Figure 2, BSE images of the indented locations at the SCI are reported. The indented locations are overlapped by a map showing the E_{cp} of each indent (divided in 5 rows and 20 columns; column #1, #5, #10, #15 and #20 of the E_{cp} map are highlighted in each Figure).
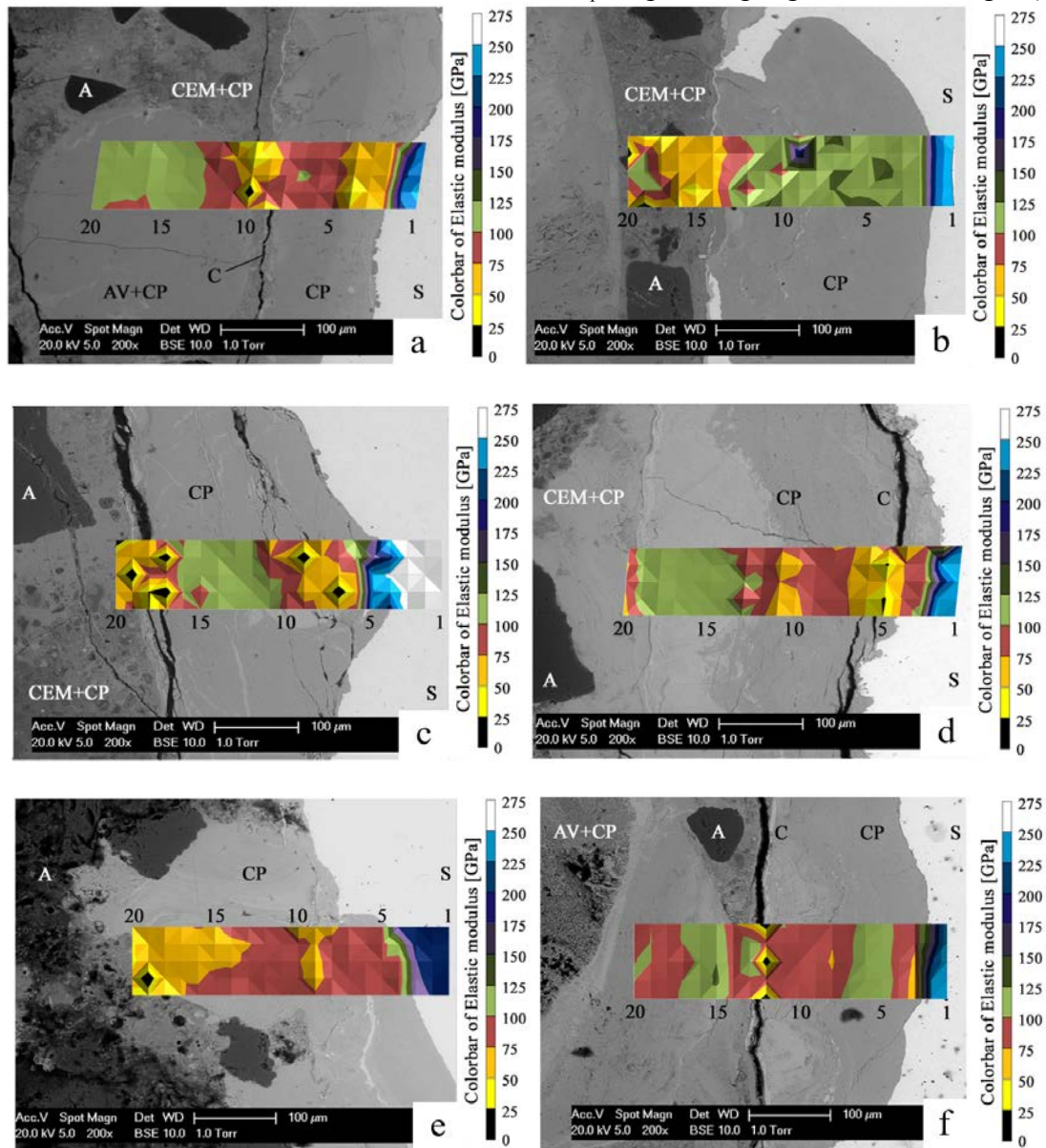

Figure 2: BSE image of indented location with overlapped E_{cp} map (S=steel; CEM=cement paste; CP=corrosion products; A=aggregate; AV=air void; C=crack). (a=1550-S1; b=1550-S3; c=2550-S3; d=3550-S2; e=5550-S1; f=5550-S2).

For 1550-S1 and 5550-S2 (Figure 2a and 2f), an air void filled by corrosion product separated by a thin cement paste interlayer (around 20 μm) is visible. A cracked alongside to this interlayer is also observed for both specimens. An interfacial void filled by corrosion product is also visible for 1550-S3 (Figure 2b), separated by a cement paste interlayer of around 80

μm. In these cases, the interlayers between interfacial air voids and the reinforcement are completely filled by corrosion products. In 2550-S3, 3550-S2 and 5550-S1 (Figure 2c, 2d and 2e, respectively) no interfacial voids are observed and corrosion products penetrated the concrete matrix for more than 100 μm. A thin and bright layer (5 to 10 μm) is visible around the reinforcement for all the specimens, which is thought to represent a mill scale layer as reported by other studies [12]. This layer was found intact around the reinforcement for 1550-S3 and 3550-S2, coincident to a crack around the steel in 1550-S1, 2550-S3 and 5550-S2, while it is not intact for 5550-S1. For 2550-S3 and 3550-S2 a cracked portion of corrosion products is visible at the steel interface, with cracks parallel to the reinforcement.

According to ESEM analysis, areas of corrosion product with different grey intensity in the BSE images (hence suggesting that corrosion products have different atomic weights on average) and E_{cp} can be distinguished. A clear example of the different micro-structure of corrosion products is visible for 3550-S2, in which three corrosion product layers are visible: a cracked portion close to the reinforcement (column 1-7), a denser dark-grey portion (column 7-13) and a compact light-grey layer close at the interface between surrounding cement paste (column 13-19). Layered corrosion products are also clearly visible for 1550-S1, 2550-S3 and 5550-S2. In 1550-S1, 2550-S3 and 3550-S2 a three-layered increase of E_{cp} from the reinforcement towards the surrounding cement paste is visible. E_{cp} ranging between 25-75 GPa at the steel interface for 2550-S3 and 3550-S1 was most likely due to the presence of visible cracks rather than due to the composition of the corrosion products themselves. More variable progress of E_{cp} was found for 5550-S2. At the steel interface E_{cp} increases from 75 GPa to 125 GPa in two distinct layers. A decrease of E_{cp} (column 12-13) is coincident to an interfacial portion of corrosion products mixed with cement paste. More further away from the reinforcement, E_{cp} decreases from 125 GPa to 75 GPa when approaching an interfacial void partially filled by corrosion products. For 1550-S3 and 5550-S1, corrosion products appear more uniform and compact, with no layered structure. Consequently, E_{cp} of undisturbed corrosion product was less variable than for the other specimens, overall ranging between 100-125 GPa and 75-100 GPa, respectively. The samples investigated do not show any systematic pattern of corrosion product layers with regard to their E_{cp} and to their appearance is visible from the steel to the surrounding cement paste.

The E_{cp} ranges between 75-125 GPa (red-green), with a few areas between 50-75 GPa (orange) visible for 1550-S1 and 5550-S1. Lower E_{cp} (0-50 GPa, black-yellow) was measured for portions of cracked corrosion products as well as for corrosion products mixed with cement paste.

4. DISCUSSION

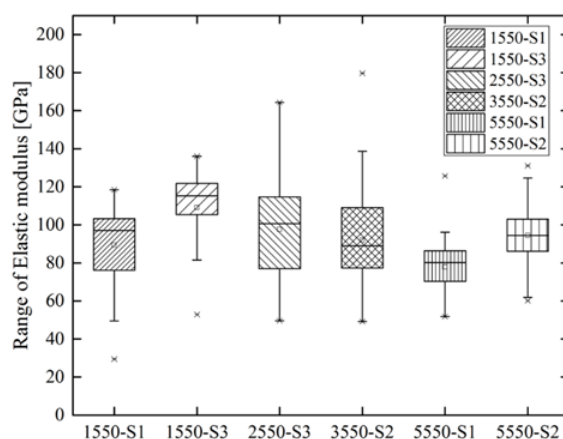In Figure 9 the range of E_{cp} measured for each specimen is reported.

Figure 3: Range of E$_{cp}$ of corrosion products per specimen. The top, middle and bottom line of the boxes correspond to the 75-, 50- and 25-percentile value (x$_{75}$, x$_{50}$ and x$_{25}$) respectively. The whiskers show the minimum and maximum values.

The range of E$_{cp}$ of undisturbed corrosion products formed in different concrete mixes does not considerably change depending on the cement type of the mixture, since average values of E$_{cp}$ between 80-100 GPa have been measured in all specimens. This range of E$_{cp}$ is similar to what was found by Hosemann et al. [12] (70-100 GPa) and slightly different from the E$_{cp}$ studied through nano-indentation by others [7-8]. Šavija et al. [8] found that E$_{cp}$ ranged between 49.4-67.9 GPa, while Zhao et al. [7] measured E$_{cp}$ of two distinct corrosion product layers. In this latter case, they found that the inner layer (formed due to degradation of the reinforcement) had E$_{cp}$ of 47-86 GPa, while the outer layer (mill scale-related) had 98-122 GPa. Differences with previous studies might be addressed to the different preparation of samples. Both of these studies investigated the E$_{cp}$ of anodically-formed corrosion products. Anodic corrosion tends to influence the formation and further distribution of corrosion products [8]. The corrosion current density at which corrosion is accelerated might influence the micro-structure of corrosion products, such as its density and crystallinity, which likely influence the resulting micro-mechanical properties. Further specimens nano-indented by Zhao et al. [7] included portions of corrosion product previously peeled from a corroding bar, thus excluding the potential effect that the steel/concrete interface might have on the corrosion product's microstructure (due to constrain from the surrounding concrete). The influence that boundary conditions (i.e. presence of cracks and cement paste) were already pointed out by Šavija et al. [8], who observed that the elastic modulus of cracked corrosion products was lower than the E$_{cp}$ of undisturbed products. This is because the presence of defects and lack of surrounding boundaries would offer accommodating area for the deformation of the material while being indented, as it was also observed in the present study. Differently to previous researches [7-8], in this study corrosion product was naturally-generated over 20 years, avoiding any potential influence of anodic acceleration of corrosion. Also, nano-indentation was performed on corrosion products still constrained by the surrounding steel and concrete, which is more representative for a real case scenario than extracted portions of corrosion product. Nevertheless, the range of E$_{cp}$ measured in this study is overall comparable to the one analysed through nano-indentation by previous studies [7, 8, 12].

In Figure 4, the relation between E_{cp} and elemental concentration (Ca, Si, Fe) resulting from EDS spot analysis is shown. During the nano-indentation test, the location that is indented might be a cluster of different components, and not corrosion product only. Higher concentrations of Ca and Si suggests that corrosion product was partially mixed with cement paste, with consequent lower concentration of Fe. In agreement with Šavija et al. [8], corrosion products mixed with cement paste have lower Elastic modulus than the E_{cp} of undisturbed corrosion product, which generally contained no more than 2 wt% of Ca and Si. Figure 4 shows that E_{cp} is proportional to the Fe concentration of corrosion products. One possible explanation might be that the Elastic modulus of the indented cluster is proportional to its inter-atomic bonding energy, which is inversely proportional the inter-atomic distance and directly proportional to the ionic valency of the cluster. Since (Fe^{III}) iron oxides have lower inter-atomic distance and higher ionic valency than CaO and SiO_2 respectively, it is reasonable to find E_{cp} rather than that of corrosion product mixed with cement paste. Zhao et al. [7] observed that E_{cp} of the mill scale layer was higher than that of electrochemical corrosion products, and they concluded that this was due to the higher Fe/O of the former one, as reported by Cook [13]. This relation was recently confirmed by Jiang et al. [14]. In principle, the results of Figure 4 might suggest the same relation. However, since significant scatter of E_{cp} with 55-65 % Fe is visible, it may be the case that E_{cp} of corrosion product layers is more precisely dependant on the mineralogy of the corrosion products (i.e. different phases or polymorphs), as widely investigated by Dehoux et al. [15].
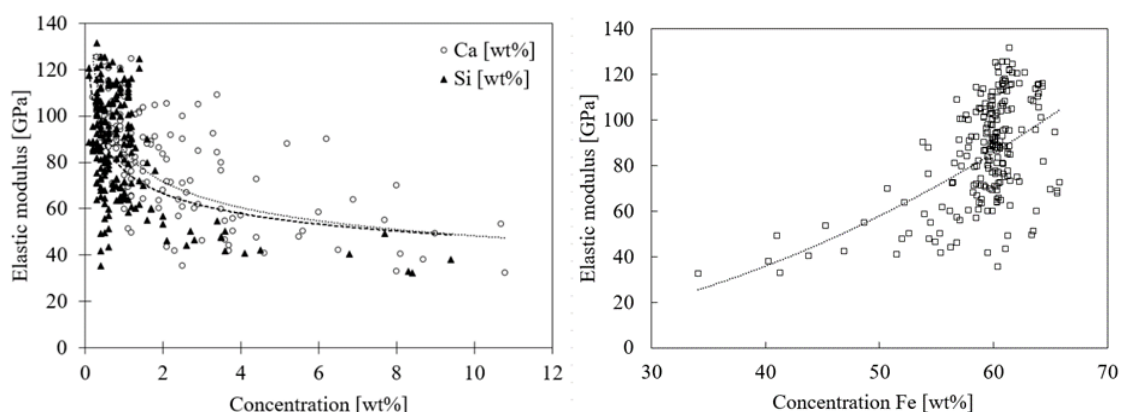

Figure 4: Influence of concentration of Ca, Si [wt.%] (left) and Fe [wt.%] (right) on E_{cp}

In line with previous studies [7, 16], corrosion products formed at the SCI were found to be made up by successive layers. Corrosion product layers for which the BSE image indicates a (slightly) different chemical composition also show different E_{cp}, as clearly visible for 1550-S1, 3550-S2 and 5550-S2. Nevertheless, the samples do not show a systematic pattern of corrosion product development from the reinforcement to the surrounding cement paste in terms of BSE appearance and E_{cp}. Through SEM and Raman spectroscopy analysis of corrosion product, both Dehoux et al. [15] and Demoulin et al. [16] found that layers of corrosion products with a different appearance under BSE were representative for different mineralogy of corrosion products. In this study, the mineralogical characterization was not carried out. It is likely, however, that differences in mineralogical composition provide an explanation for the different ranges of E_{cp}.

5. CONCLUSIONS

- From nano-indentation tests on natural corrosion products generated over 20 years due to chlorides, an average E_{cp} ranging between 80-100 GPa is obtained for use in numerical models for corrosion induced cover cracking. On average, no significant variations have been observed between E_{cp} of corrosion products generated in mixes cast with different cement types (CEM I, II/B-V, III/B and V/A).
- E_{cp} of corrosion products determined in this study is overall comparable to the E_{cp} found in previous studies in which nano-indentation was performed [7-8, 12, 14-15]. Slight differences with previous studies might be due to the different preparation of the samples and of the test set-ups. Nevertheless, the order of magnitude of E_{cp} is overall comparable to the one proposed by other authors.
- No systematic pattern of corrosion product layers from the reinforcement towards the surrounding cement paste with regard to its appearance and Elastic modulus was found.
- EDS spot analysis revealed that E_{cp} is inversely proportional to the presence of cracks and the concentration of cement-related components (i.e. Ca and Si). Furthermore, corrosion products with higher concentration of Fe show higher E_{cp}.

REFERENCES

[1] Bertolini L, Elsener B, Pedeferri P, Redaelli E, Polder RB (2013). Corrosion of steel in concrete: prevention, diagnosis, repair. JohnWiley & Sons.

[2] Bazant Z (1979) Physical model for steel corrosion in concrete sea structures—theory. J Struct Div ASCE 105(6):1137–1153.

[3] Molina J, Alonso C, Andrade C (1993) Cover cracking as a function of rebar corrosion: Part 2—Numerical model. Mater Struct 26:532–548.

[4] Liu Y, Weyers RE (1998) Modeling the time-to-corrosion cracking in chloride contaminated reinforced concrete structures. ACI Mater J 95(6):675–680.

[5] Ozbolt J, Orsanic F, Balabanic G, Kuster M (2013) Modeling damage in concrete caused by corrosion of reinforcement: coupled 3D FE model. Int J Fract 178(1–2): 233–244.

[6] Savija B, Lukovic M, Pacheco J, Schlangen E (2013) Cracking of the concrete cover due to reinforcement corrosion: a two-dimensional lattice model study. Constr Build Mater 44:626–638.

[7] Zhao Y, Dai H, Jin W (2012). A study of the elastic moduli of corrosion products using nanoindentation techniques. Corros Sci 65:163-168.

[8] Savija B, Lukovic M, Hosseini SAS, Pacheco J, Schlangen E (2015). Corrosion induced cover cracking studied by X-ray computed tomography, nanoindentation and energy dispersive X-ray spectrometry (EDS). Mater. Struct. 48 (2043-2062).

[9] Polder RB, Russo P (1998) Concrete resistivity, corrosion potential and corrosion rate at young age as a function of cement type. 98-BT-R1664. TNO Building and Construction Research. Rijswijk, TNO.

[10] Rossi E, Nijland T, Çopuroğlu O, Polder RB, Šavija B. (2019). The influence of defects at the steel/concrete interface for pitting corrosion initiation studied through X-ray Computed Tomography and image analysis. In MATEC Web of Conferences (Vol. 289, p. 10011). EDP Sciences.

[11] Oliver WC, Pharr GM (2004) Measurement of hardness and elastic modulus by instrumented indentation: advances in understanding and refinements to methodology. J Mater Res 19:3–20.

[12] Hosemann P, Swadener JG, Welch J, Li N (2008). Nano-indentation measurement of oxide layers formed in LBE on F/M steels. J. Nucl. Mater. 201-205.

[13] Cook DC (2005). Spectroscopic identification of protective and non-protective corrosion coatings on steel structures in marine environments. Corros. Sci. 2250-2570.

[14] Jiang B, Doi K, Tsuchiya K, Kawano Y, Kori A, Ikushima K (2019). Micromechanical properties of steel corrosion products in concrete studied by nano-indentation technique. Corros. Sci.

[15] Dehoux A, Bouchelaghem F, Berthaud Y (2015). Micromechanical and microstructural investigation of steel corrosion layers of variable age developed under impressed current method, atmospheric or saline conditions. Corrosion Science 97:49-61.

[16] Demoulin A, Trigance C, Neff D, Foy E, Dillmann P, L'Hostis V (2010). The evolution of the corrosion of iron in hydraulic binders analysed from 46- and 260-year-old buildings. Corrosion Science 52:3168–3179.